Wave Motion 51 (2014) 1138–1148

Contents lists available at ScienceDirect

Wave Motion

journal homepage: www.elsevier.com/locate/wavemoti

Nonlinear elastic effects in graphite/epoxy: An analytical and numerical prediction of energy flux deviation

Arun K. Nair [a,*], Ronald D. Kriz [a], William H. Prosser [b]

[a] Department of Engineering Science and Mechanics, Norris Hall, Room 300-C, Virginia Tech, Blacksburg, VA-24061, United States
[b] NASA Langley Research Center, Hampton, VA-23681, United States

HIGHLIGHTS

- Applying external load to graphite/epoxy changes its anisotropy.
- Using acoustoelastic theory we predict the energy flux shift for QL, QT and PT waves.
- We predict the energy flux shift for QT wave is higher for shear compared to normal load.
- Finite element simulations validate acoustoelastic theory predictions.

ARTICLE INFO

Article history:
Received 16 July 2013
Received in revised form 5 June 2014
Accepted 12 June 2014
Available online 26 June 2014

Keywords:
Acoustoelastic effects
Composite material
Energy flux deviation
Stress induced anisotropy
Finite element method

ABSTRACT

Manipulating acoustic wave propagation through a material have several interdisciplinary applications. Here we predict shift in energy flux deviation for acoustic waves propagating in unidirectional graphite/epoxy due to applied normal and shear stresses using both an analytical model, using acoustoelastic continuum theory, and a finite element discrete numerical model. The acoustoelastic theory predicts that the quasi-transverse (QT) wave exhibits larger shifts in energy flux deviation compared to quasi-longitudinal (QL) or the pure transverse (PT) due to an applied shear stress for fiber orientation angle ranging from 0° to 60°. Due to an applied shear stress the QT wave exhibits a shift in energy flux deviation at 0° fiber orientation angle as compared to normal stress case where the flux deviation and its load induced shift are both zero. A finite element model (FEM) is developed where equations of motion include the effect of nonlinear elastic coefficients. Element equations were integrated in time using Newmark's method to determine the shift in energy flux deviations in graphite/epoxy for different loading cases. The energy flux shift of QT waves predicted by FEM for fiber orientation angles from 0° to 60° for applied shear stress case is in excellent agreement with acoustoelastic theory. Because energy shift magnitudes are not small, it is possible to experimentally measure these shifts and calibrate shifts with respect to load type (normal/shear) and magnitude.

1. Introduction

Recent developments in guiding and magnifying acoustic wave propagation through a medium and their application to engineering have invoked tremendous interest among the scientific community. Developments of acoustic metamaterials

* Correspondence to: Department of Mechanical Engineering, 863 West Dickson Street, University of Arkansas, Fayetteville, AR-72701, United States. Tel.: +1 479 575 2573; fax: +1 479 575 6982.
E-mail address: nair@uark.edu (A.K. Nair).

http://dx.doi.org/10.1016/j.wavemoti.2014.06.002
0165-2125/

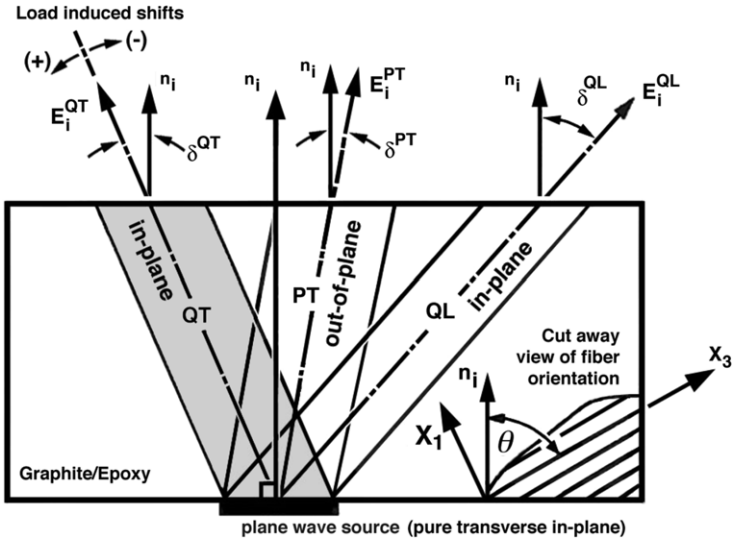

Fig. 1. Wave types (QT, QL, PT), energy flux propagation directions, E_i, and in-plane co-ordinate axes, x_1–x_3, defined with respect to fiber orientation for a unidirectional graphite/epoxy composite.

have proven to act as hyperlenses for several applications in non-destructive material testing and medical ultra-sound imaging [1–3]. In these studies, the anisotropy of the material is the governing factor in guiding the wave propagation. Several studies [4–7] have shown that acoustic cloaking can be achieved by controlling the microstructure of the material. These studies indicate that by changing the anisotropy of the material, the acoustic waves can be guided through a material. Acoustic wave propagation has interdisciplinary applications and is a widely used technique in engineering and medical sciences [8–10]. In this paper, we show how the anisotropy changes due to an externally applied load to a fiber reinforced composite material, which in turn can be used to control the acoustic wave propagation direction.

In an anisotropic material, the direction of energy flux (energy per unit time per unit area) of an ultrasonic plane wave deviates from the intended direction of propagation as compared to an isotropic material, where the energy flux propagates in a direction parallel to the wave front normal vector, n_i, see Fig. 1. This phenomenon, exhibited by linear elastic anisotropic materials, is known as the energy flux deviation. The elastic coefficients of the material influence the energy flux deviation [11,12]. Energy flux deviation was experimentally observed in quartz crystals [11,13] and unidirectional graphite fiber reinforced epoxy [14,15].

Nonlinear elastic behavior is generally neglected in ultrasonic wave propagation due to small strains (or small amplitude) imposed on the sample; however this effect can be predominant in three cases of wave propagation as pointed out by Green [13]. First, the amplitude of the wave may be large enough to cause finite strains in the material. In the second case nonlinear behavior occurs when a small amplitude wave is superimposed on a large external static stress, and finally nonlinear effects caused by defects in the material. In this paper the second case of nonlinear effects is studied for measurable shifts in energy flux deviations of waves propagating in graphite/epoxy. Tokuoka and Iwashimizu [16] derived the Christoffel equation for an anisotropic material under stress assuming hyperelasticity using plane wave solution. Man and Lu [17] later extended the applicability of Christoffel equation to general types of loading history and plastic deformations. Prosser et al. [18] studied graphite/epoxy for applied stress along fiber axis and laminate stacking direction using acoustoelastic theory and measured the flux deviation angle. Using Man and Lu's theory [17] Degtyar and Rokhlin [19] derived in detail the equation of motion due to wave propagation superimposed on a prestressed solid and also studied the elastic wave propagation between two generally anisotropic stressed solids as well as stressed solid and fluid for different materials [20]. Zhuk and Guz [21] studied nanocomposite material with prestress, where the nonlinearity was described by the Murnaghan potential. Similarly, Parnell [22] used asymptotic homogenization theory in the deformed configuration to find the effective response of a prestressed nonlinear elastic composite bar. The flux shift is also observed in graphite/epoxy due to the moisture absorption by the matrix or fiber degradation [23]. A recent study involving experiments and simulations show that stress wave trajectory can be controlled [24] by the anisotropy of the material. Even though Prosser et al. [18] studied shifts in energy flux deviations due to normal stress effects on graphite/epoxy, the flux deviation due to shear stress was left unexplored.

In this paper, we study the effect of nonlinear elasticity on shifts in energy flux deviation in unidirectional graphite/epoxy due to applied normal and shear stresses. Due to elastic nonlinearity the angle of flux deviation can be measured as a function of applied stresses. We model the energy flux deviation using acoustoelastic theory [17] and the flux shift, which is the difference between flux deviation angle due to applied stress and the flux deviation due to zero stress state, is compared for different stresses. Finite element equations are derived for equation of motion containing nonlinear elastic coefficients, C_{ijklmn}, and integrated in time using Newmark's method. We predict the energy flux shift for quasi-transverse (QT) wave using finite element method (FEM) for fiber angle orientations ranging from 0° to 60° and then compare with acoustoelastic

theoretical predictions for the applied shear stress case. The results from this study demonstrate that load induces significant shifts in energy flux deviations that can be experimentally verified when a shear stress greater than 0.1 GPa is applied to unidirectional graphite/epoxy over a range of fiber orientations.

2. Theory

Elastic wave propagation in solids can be described in mathematical form as a function of stiffness coefficients of the material and the spatial and time derivatives of displacement. In this section, the analytical formulation of the stress-induced anisotropy is introduced and how it is incorporated into the wave equation is presented. Based on the analytical model, the derivation of the finite element equations is shown along with the time integration methodology.

2.1. Analytical formulation

The energy flux vector E_j associated with planar waves is related to the elastic stiffness coefficients C_{ijkl} and the spatial and time derivatives of displacement vector u_i by the following equation [11,12].

$$E_j = -C_{ijkl}\left(\frac{\partial u_k}{\partial x_l}\right)\left(\frac{\partial u_i}{\partial t}\right) \tag{1}$$

Here we use acoustoelastic theory to include the nonlinear elastic properties on the energy flux deviation. According to acoustoelastic theory, the applied stress σ_{ij} changes the linear elastic coefficients to give an effective linear stiffness tensor using the following relation [25].

$$C^*_{nlij} = K_{nlij} + \sigma_{lj}\delta_{ni} \tag{2}$$

where C^*_{nlij} is the effective linear stiffness tensor, σ_{lj} is the applied stress, δ_{ni} is Kronecker delta. Due to the applied stress, the effective stress tensor C^*_{nlij} lacks full symmetry (relative to permutation between the index pairs n, l and i, j), however shows the following symmetry $C^*_{nlij} = C^*_{ijnl}$ [25]. The second order tensor K_{nlij} is defined [18] as a function of C_{ijklmn} (third order stiffness tensor).

$$\begin{aligned} K_{nlij} = {} & C_{nlij} + C_{rlij}\varepsilon_{nr} + C_{nsij}\varepsilon_{ls} + C_{nlpj}\varepsilon_{ip} + C_{nliq}\varepsilon_{jq} + C_{nlijuv}\varepsilon_{uv} \\ & + C_{rlijuv}\varepsilon_{uv}\varepsilon_{nr} + C_{nsijuv}\varepsilon_{uv}\varepsilon_{ls} + C_{nlpjuv}\varepsilon_{uv}\varepsilon_{ip} + C_{nliquv}\varepsilon_{uv}\varepsilon_{jq} \end{aligned} \tag{3}$$

In Eq. (3) C_{nlij} is the linear elastic coefficient, C_{nlijuv} is the nonlinear elastic coefficient, which is also known as third order stiffness coefficient with respect to the strain energy function, and ε_{nr} is the strain resulting from the applied stress σ_{ij}. The third order stiffness tensor has the following symmetry relations $C_{nlijuv} = C_{lnjuv} = C_{ijnluv} = C_{uvijnl}$ [20]. Our analysis shows that the inclusion of third order elastic constants can change the effective stiffness tensor for graphite/epoxy by ± 0.9 GPa. The strain can be found as the product of compliance tensor (inverse of C_{nlij}) and the applied stress. The K_{nlij} tensor is composed of ten terms, five linear terms and five nonlinear terms. Eq. (2) has nine nonzero terms when normal stresses are applied and shear stresses are zero. The inclusion of shear stress terms will lead to an additional eighteen terms. This is too cumbersome to expand by hand and solve, hence we use a computer program to compute all of the terms used to determine C^*_{nlij} tensor. For example if C^*_{nlij} is nonsymmetric with 81 independent terms and each of these terms is the sum of 27 terms, the total number of terms is 2187. Previous investigations [18] have looked into normal stress cases and general stress states.

Eq. (1) can now be written as

$$E_j = -\sigma'_{ij}\left(\frac{\partial u_i}{\partial t}\right); \quad \text{where } \sigma'_{ij} = C^*_{ijkl}\varepsilon'_{kl} \tag{4}$$

where σ'_{ij} is the stress and ε'_{kl} the strain due to the wave propagation. The Christoffel equation for the wave propagation in terms of the effective linear elastic coefficient assuming a plane periodic solution can be written as [16,19,26]

$$(C^*_{ijkl}l_l l_j - \rho v^2\delta_{ik})\alpha_k = 0 \tag{5}$$

where C^*_{ijkl} is the effective linear stiffness tensor, l_l is the direction cosine of the wave normal, δ_{ik} is Kronecker delta and α_k is the eigenvector or the direction cosine of particle displacement vector corresponding to each eigenvalue ρv^2 (ρ is density and v is velocity). The energy from Eq. (4) is time averaged over one cycle to get $\overline{E_i}$, where $\overline{E_i} = \sigma'_{ik}\alpha_k$. The total energy over one cycle is defined as $\overline{E}_T^2 = \overline{E}_1^2 + \overline{E}_2^2 + \overline{E}_3^2$, hence the direction cosines of energy flux vector is given as $a = \frac{\overline{E_1}}{\overline{E_T}}$, $b = \frac{\overline{E_2}}{\overline{E_T}}$ and $c = \frac{\overline{E_3}}{\overline{E_T}}$.

The flux deviation angle (δ) in Fig. 1 is computed as the difference between the angle (θ) that energy flux vector makes with the x_3 axis and the wave normal vector (n_i) makes with respect to the x_3 axis. Mathematically, the flux deviation angle (δ) can be represented as follows:

$$\delta = \tan^{-1}((\tan\beta - \tan\theta)/(1 + \tan\beta\tan\theta)) \tag{6}$$

where $\tan(\beta) = a/c$ is defined in terms of the direction cosines of energy flux vector. A positive flux deviation corresponds to deviation of energy towards the left hand side of the wave normal n_i as shown in Fig. 1.

2.2. Finite element formulation

In order to confirm the flux deviation angles predicted by acoustoelastic theory, the finite element method [27] along with Newmark's method [28] in time is used to solve the equations of motion at each time step. The equation for small elastic motion due to wave propagation superimposed on a prestressed state in the absence of body forces can be written as

$$\sigma'_{ij,j} = \rho u_{i,tt} \tag{7}$$

where σ'_{ij} is the stress defined by Eq. (4), ρ is the density and u_i is the displacement as a result of wave propagation in the material. The weak form [29] is constructed by multiplying Eq. (7) by arbitrary functions which represent virtual displacements δu_i.

$$\int_V \delta u_i(\sigma'_{ij,j} - \rho u_{i,tt})dV = 0 \tag{8}$$

Integrating the above equations by parts and using divergence theorem gives the weak form of the governing equations as follows

$$0 = \int_V (\sigma'_{ij}\delta\varepsilon_{ij} + \delta u_i \rho u_{i,tt})dV - \oint_S (\sigma'_{ij} n_j \delta u_i)dS \tag{9}$$

Substituting $\sigma'_{ij} = C^*_{ijkl}\varepsilon'_{kl}$, and assuming plain strain conditions ($\frac{\partial u_2}{\partial x_1} = \frac{\partial u_2}{\partial x_2} = \frac{\partial u_2}{\partial x_3} = \frac{\partial u_1}{\partial x_2} = \frac{\partial u_3}{\partial x_2} = 0$), Eq. (9) can be written over the domain Ω as

$$\begin{aligned}\int_\Omega \Bigg\{ &\frac{\partial \delta u_1}{\partial x_1}\left[C^*_{1111}\frac{\partial u_1}{\partial x_1} + C^*_{1113}\frac{\partial u_1}{\partial x_3} + C^*_{1131}\frac{\partial u_3}{\partial x_1} + C^*_{1133}\frac{\partial u_3}{\partial x_3}\right] \\ &+ \frac{\partial \delta u_1}{\partial x_3}\left[C^*_{1311}\frac{\partial u_1}{\partial x_1} + C^*_{1313}\frac{\partial u_1}{\partial x_3} + C^*_{1331}\frac{\partial u_3}{\partial x_1} + C^*_{1333}\frac{\partial u_3}{\partial x_3}\right] + \delta u_1 \rho \frac{\partial^2 u_1}{\partial t^2}\Bigg\} dx_1 dx_3 - \int_\Gamma (\delta u_1 t_1 n)dS = 0\end{aligned} \tag{10}$$

$$\begin{aligned}\int_\Omega \Bigg\{ &\frac{\partial \delta u_3}{\partial x_1}\left[C^*_{3111}\frac{\partial u_1}{\partial x_1} + C^*_{3113}\frac{\partial u_1}{\partial x_3} + C^*_{3131}\frac{\partial u_3}{\partial x_1} + C^*_{3133}\frac{\partial u_3}{\partial x_3}\right] \\ &+ \frac{\partial \delta u_1}{\partial x_3}\left[C^*_{3311}\frac{\partial u_1}{\partial x_1} + C^*_{3313}\frac{\partial u_1}{\partial x_3} + C^*_{3331}\frac{\partial u_3}{\partial x_1} + C^*_{3333}\frac{\partial u_3}{\partial x_3}\right] + \delta u_3 \rho \frac{\partial^2 u_3}{\partial t^2}\Bigg\} dx_1 dx_3 - \int_\Gamma (\delta u_3 t_3 n)dS = 0\end{aligned} \tag{11}$$

Eqs. (10) and (11) represent the weak formulation of the equation of motion in the x_1 and x_3 directions. Finite element approximations are sought for displacements u_1 and u_3 assuming that the dependence of displacement on time is separated from the dependence on x_1 and x_3 directions. The approximations take the form,

$$u_1(x_1, x_3, t) = \sum_{j=1}^{n} U_j(t)\Gamma_j^{u_1}(x_1, x_3), \qquad u_3(x_1, x_3, t) = \sum_{j=1}^{n} W_j(t)\Gamma_j^{u_3}(x_1, x_3) \tag{12}$$

where, Γ_j represents the shape functions, which are continuous in the sub-domain of the problem over an element. The selection of the shape functions [27] or interpolation functions are made in such a way that the displacements are continuous across the boundary of each element of the finite element mesh and other conditions demanded by the variational form. The coefficients of the approximating functions are the nodal displacement values in each element node. Substituting these approximations into the weak form Eqs. (10) and (11) and the collection of coefficients of variations of displacements and placing them in matrix form will give the following matrix equations.

$$\begin{bmatrix}[M^{u_1u_1}][0] \\ [0][M^{u_3u_3}]\end{bmatrix}\begin{Bmatrix}\{\ddot{u_1}\} \\ \{\ddot{u_3}\}\end{Bmatrix} + \begin{bmatrix}[K^{u_1u_1}][K^{u_1u_3}] \\ [K^{u_3u_1}][K^{u_3u_3}]\end{bmatrix}\begin{Bmatrix}\{u_1\} \\ \{u_3\}\end{Bmatrix} = \begin{Bmatrix}\{f^{u_1}\} \\ \{f^{u_3}\}\end{Bmatrix} \tag{13}$$

where M is the mass matrix, K is the stiffness matrix, f is the force vector and u and w are the displacements in the x_1 and x_3 directions. Each sub matrix in Eq. (13) is defined as follows

$$M_{ij}^{u_1u_1} = \int_\Omega [\rho\Gamma_i^{u_1}\Gamma_j^{u_1}]dx_1dx_3 \tag{14}$$

$$M_{ij}^{u_3u_3} = \int_\Omega [\rho\Gamma_i^{u_3}\Gamma_j^{u_3}]dx_1dx_3 \tag{15}$$

$$K_{ij}^{u_1u_1} = \int_\Omega \left(C^*_{1111}\frac{\partial\Gamma_i}{\partial x_1}\frac{\partial\Gamma_j}{\partial x_1} + C^*_{1113}\frac{\partial\Gamma_i}{\partial x_1}\frac{\partial\Gamma_j}{\partial x_3} + C^*_{1311}\frac{\partial\Gamma_i}{\partial x_3}\frac{\partial\Gamma_j}{\partial x_1} + C^*_{1313}\frac{\partial\Gamma_i}{\partial x_3}\frac{\partial\Gamma_j}{\partial x_3}\right)dx_1dx_3 \tag{16}$$

$$K_{ij}^{u_1u_3} = \int_\Omega \left(C^*_{1131}\frac{\partial\Gamma_i}{\partial x_1}\frac{\partial\Gamma_j}{\partial x_1} + C^*_{1133}\frac{\partial\Gamma_i}{\partial x_1}\frac{\partial\Gamma_j}{\partial x_3} + C^*_{1331}\frac{\partial\Gamma_i}{\partial x_3}\frac{\partial\Gamma_j}{\partial x_1} + C^*_{1333}\frac{\partial\Gamma_i}{\partial x_3}\frac{\partial\Gamma_j}{\partial x_3}\right)dx_1dx_3 \tag{17}$$

$$K_{ij}^{u_3u_1} = \int_{\Omega} \left(C^*_{3111} \frac{\partial \Gamma_i}{\partial x_1} \frac{\partial \Gamma_j}{\partial x_1} + C^*_{3113} \frac{\partial \Gamma_i}{\partial x_1} \frac{\partial \Gamma_j}{\partial x_3} + C^*_{3311} \frac{\partial \Gamma_i}{\partial x_3} \frac{\partial \Gamma_j}{\partial x_1} + C^*_{3313} \frac{\partial \Gamma_i}{\partial x_3} \frac{\partial \Gamma_j}{\partial x_3} \right) dx_1 dx_3 \tag{18}$$

$$K_{ij}^{u_3u_3} = \int_{\Omega} \left(C^*_{3131} \frac{\partial \Gamma_i}{\partial x_1} \frac{\partial \Gamma_j}{\partial x_1} + C^*_{3133} \frac{\partial \Gamma_i}{\partial x_1} \frac{\partial \Gamma_j}{\partial x_3} + C^*_{3331} \frac{\partial \Gamma_i}{\partial x_3} \frac{\partial \Gamma_j}{\partial x_1} + C^*_{3333} \frac{\partial \Gamma_i}{\partial x_3} \frac{\partial \Gamma_j}{\partial x_3} \right) dx_1 dx_3 \tag{19}$$

Due to certain symmetry properties of C^*_{ijkl} tensor under applied stress, the resulting FEM elemental stiffness matrix K is symmetric.

2.2.1. Integration in time

The Newmark's constant average-acceleration method is used to compute the displacements for each time step. This is an extremely well-known method, and its application for solving wave equation can be found in Refs. [28,30]. It is sufficient to state that the generic velocity component $\dot{U}$ and displacement component U for time $t + \Delta t$ are assumed to possess the forms

$$\dot{U}^{t+\Delta t} = \dot{U}^t + [(1-\delta)\ddot{U}^t + \delta \ddot{U}^{t+\Delta t}]\Delta t \tag{20}$$

$$U^{t+\Delta t} = U^t + \dot{U}^t \Delta t + \left[\left(\frac{1}{2} - \alpha \right) \ddot{U}^t + \alpha \ddot{U}^{t+\Delta t} \right] \Delta t^2 \tag{21}$$

The selection of constants $\delta = 0.5$ and $\alpha = 0.25$ provides unconditional stability to the problem. The equilibrium equation at time $t + \Delta t$ can be written as

$$M\ddot{U}^{t+\Delta t} + C\dot{U}^{t+\Delta t} + KU^{t+\Delta t} = R^{t+\Delta t} \tag{22}$$

Here M is mass matrix, C damping matrix, K the stiffness matrix, $\ddot{U}$ the acceleration vector, $\dot{U}$ the velocity vector, U the displacement vector, and R is the load vector for time $t + \Delta t$. From Eqs. (20) and (21), the accelerations and velocity can be written in terms of unknown displacements alone. This relation is then substituted into (22) to compute the displacements. The initial acceleration vector is evaluated using the initial conditions, and the analysis proceeds in stepwise fashion as each of the fields is updated at the end of the specified time step.

3. Simulation setup and validation

3.1. Analytical

Here we assume that the graphite/epoxy is transversely isotropic for computing the flux deviation angle at different stress states. The x_3 axis is taken as the fiber orientation axis and x_1 axis the laminate stacking direction. A positive flux deviation is defined as the energy flux deviation from the wave normal n_i to the left side; while a negative flux deviation implies that the energy deviates towards the right side of n_i axis, Fig. 1. The elastic linear and nonlinear coefficients for graphite/epoxy are listed in Tables 1 and 2. In both tables, tensor notation is replaced with contracted Voigt notation.

An in-house computer code is used to compute the flux deviation angles (Eq. (6)) for the zero stress state and applied normal and shear stress states from 0° to 60° fiber orientation. In all cases, the flux shifts are calculated for fibers oriented from 0° to 60° at intervals of 10°. First we validate the flux deviation angles for in-plane quasi-longitudinal (QL) and quasi-transverse (QT) waves, and out-of-plane pure-transverse (PT) waves under zero stress state with Prosser et al. [18] and Kriz and Heyliger [31], then we compute the flux shift of QT, QL and PT waves for an applied shear stress of 0.1 GPa in the x_1–x_3 plane. In order to study the effect of shear stress in flux shift, the flux shift is calculated at different shear stresses. Finally, a comparison of flux shift is carried out with normal stress of 0.1 GPa along x_1 axis and 1.0 GPa along x_3 axis.

3.2. Finite element simulation

The finite element equation of motion derived in Section 2.2 is solved by a computer code generated in FORTRAN to study stress-induced shifts in energy flux deviations. The computation of energy flux deviation, and stress-induced shifts, is then carried out for both zero stress state and applied shear stress state for each 10° interval of fiber orientation angle. In this section, we first discuss the dispersion effects when using a finite element method for wave propagation and then validate the FEM code for a 2-D graphite/epoxy plate under zero stress state.

3.2.1. Dispersion of waves

When using finite elements to model wave propagation, numerical dispersion is observed when wave velocity is a function of the number of finite elements contained within the wavelength of a propagating wave. Here the study of dispersion in unidirectional graphite/epoxy is carried out, which has a transversely isotropic symmetry and is highly anisotropic. The objective is to study the effect of anisotropy on the flux deviation (group velocity) propagation direction as a function of different unidirectional fiber orientations, 0° to 60°.

Table 1
Linear elastic coefficients [15].

C_{ij} (GPa)	
C_{11}	14.26
C_{12}	6.78
C_{13}	6.5
C_{33}	108.4
C_{44}	5.27

Table 2
Third order (nonlinear) elastic coefficients [15].

C_{ijk} (GPa)	C_{111}	C_{112}	C_{113}	C_{123}	C_{144}	C_{155}	C_{344}	C_{133}	C_{333}
	−214	−89	−4	6.5	−33.4	−49.1	−47	−243	−325

In general, the energy flux associated with the actual wave "group" velocity deviates from the wave "phase" velocity, which is associated with normal to the plane wave front, n_i. Between 0° and 90°, the group velocity deviates from the phase velocity and the energy associated with the wave initially launched at the boundary as an in-plane pure transverse (T) wave bifurcates into an in-plane quasi-transverse (QT) and in-plane quasi-longitudinal (QL) waves. No energy associated with the in-plane pure transverse (T) wave at the boundary is transferred to the out-of-plane pure-transverse (PT) wave. At 0° and 90° fiber orientations the group and phase velocities are the same. This case is used here for simplicity to study dispersion of in-plane pure transverse (T) waves prior to studying dispersion at various fiber orientations.

We use a 60 × 30 mesh for this study with four-noded isoparametric elements. Increasing the number of elements at the boundary transducer results in an increase in the number of elements contained in the T wave that is launched at the boundary. For 12, 16, 20 and 24 elements per wavelength, we observe 3, 4, 5, and 6 elements respectively contained within the propagating T wave. Another important observation is the increasing wave velocity with increasing number of elements per wavelength contained in the propagating T wave. This is expected since larger number of elements contained in a propagating wave approach the ideal case of a wave propagating in a non-dispersive continuum. With only 4 elements per wavelength the propagating T wave is altered by the FEM mesh, which has a group velocity of zero, which demonstrates significant dispersion. Dispersion is minimized but still exists even at 24 elements per wavelength at the boundary. However 24 elements per wavelength will require larger FEM meshes where QT waves are predicted to deviate as much as 25° to the left. The numerical dispersion is an artifact of the element size used and could be eliminated by further decreasing the element size. As in most cases when modeling complex phenomena simplifying approximations are necessary and results must be interpreted within these approximations. A detailed description of this phenomenon along with animations of FEM simulations can be found at [32].

3.2.2. Stress waves in graphite/epoxy

In order to check the validity of the code for anisotropic material, the behavior of stress waves in a graphite/epoxy plate is studied and results are compared with Kriz and Heyliger [31] and Nair and Heyliger [30]. A rectangular orthotropic plate of graphite/epoxy is oriented in the x_1–x_3 plane ("in-plane") with the fibers oriented at an angle of θ from the vertical direction, Fig. 1. The plate displacements are fixed to zero along the vertical boundaries in Fig. 1, while the other two horizontal boundaries are traction-free. We use rectangular mesh comprising of 4050 four-noded isoparametric elements in total with 90 elements along the horizontal boundary and 45 elements along the vertical boundary. The parameters for the constant-average acceleration Newmark method are $\delta = 0.5$ and $\alpha = 0.25$, and density of graphite/epoxy is taken as 1610 kg/m^3. We use 24 elements per wavelength to simulate a transducer along the lower horizontal boundary and 20 time increments per wave period without inducing significant discretization errors and also to reduce wave dispersion effects. One cycle sinusoidal displacements were imposed in the horizontal direction ("in plane pure transverse") at 25 consecutive nodes along the lower horizontal boundary of the plate for a time period of 2×10^{-05} s (with a frequency of 50,000 cycles/s). The material properties used were those of graphite epoxy under zero stress state and are given in Table 3.

When the nodes of the simulated transducer are displaced horizontally (pure transverse in-plane) along the lower horizontal boundary, energy is distributed into both QT and QL waves, however parametric studies show that if nodes are constrained in the x_1–x_3 plane and displaced in the direction predicted by the eigenvector solution of Christoffel's equation, energy can be preferentially fluxed exclusively into the QT wave with no energy transferred to the QL wave. This is important because acoustoelastic theory predicts larger flux shifts for the QT wave (see Section 4) under an applied shear stress state.

4. Results and discussions

In this paper, we predict the shift in energy flux deviation of elastic waves propagating through graphite/epoxy due to an applied shear stress using acoustoelastic continuum theory and a discrete FEM model. Fig. 2 shows the flux deviation angle for zero stress predicted using acoustoelastic theory. All three wave forms QL, QT and PT exhibit flux deviation due

Table 3
Material properties used for finite element simulation.

C^*_{ijkl} (GPa)	Zero stress state	Applied shear stress of 0.1 GPa
C^*_{1111}	14.26	14.23
$C^*_{1113} = C^*_{1311}$	0	−0.54
$C^*_{3113} = C^*_{1331}$	5.27	5.24
$C^*_{1131} = C^*_{3111}$	0	−0.64
$C^*_{1133} = C^*_{3311}$	6.5	6.47
$C^*_{1333} = C^*_{3313}$	0	0.30
$C^*_{1313} = C^*_{3131}$	5.27	5.24
$C^*_{3133} = C^*_{3331}$	0	0.40
C^*_{3333}	108.4	108.37

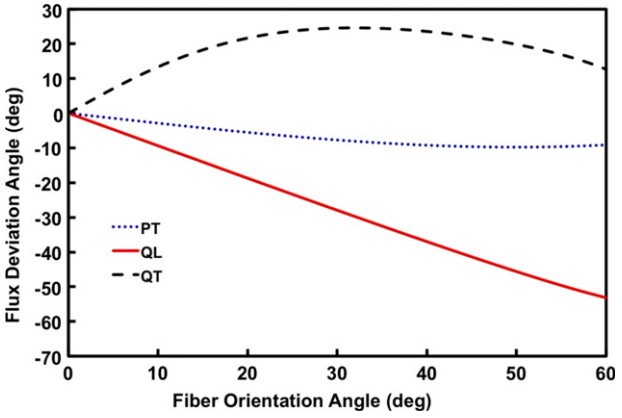

Fig. 2. Energy flux deviation angle of QL, QT and PT waves in graphite/epoxy with respect to fiber orientation angle under no applied stress shows that QL and QT waves have more flux deviation compared to PT wave.

to the anisotropy of graphite/epoxy. QL and QT has more flux deviation as compared to PT. These results are in excellent agreement with that of Kriz and Ledbetter [33] and Prosser et al. [18]. In order to study the effect of normal stress on energy flux deviation, first a normal stress of 0.1 GPa is applied along the x_1 axis and then the flux shift due to each stress is computed with respect to the fiber orientation angle. We find that the QT wave exhibits the largest load induced energy flux shift due to an applied normal stress along the x_1 axis while QL and PT exhibits small flux shift, this is consistent with [18], thus expressing confidence in our methodology and results that follows.

We then apply a shear stress of 0.1 GPa in the x_1–x_3 plane ("in-plane") in order to find the energy flux shift of QL, QT and PT as a function of fiber orientation angle (Fig. 3). It is obvious from Fig. 3 that QT has the most flux shift, while QL and PT have flux shifts close to zero. The QT wave has a 6.73° flux shift at 0° due to the applied shear stress as compared with applied normal stresses, which has zero flux shift at 0° (see Fig. 4). The nonzero flux shift at 0° due to the shear stress is the result of the shear strain that is induced in the material. Unlike the strains caused by normal stresses, this small shear strain affects the particle vibration in the direction of the flux shift. A comparison is done for the flux shift of QT wave for normal stress of 0.1 GPa along x_1 axis and 1.0 GPa along x_3 axis with a shear stress of 0.1 GPa (Fig. 4) in the x_3–x_1 plane. Results from Fig. 4 indicate the flux shift in QT wave due to the shear stress is larger than that of the normal stress cases. The higher flux deviation of QT wave due to the shear stress compared to that of normal stress could be explained by the fact that the effective stiffness tensor C^*_{nlij} has more components (see Appendix and Table 3) associated with the shear stress than normal stress, which in turn changes the anisotropy of graphite/epoxy. Moreover the values of these components are higher (more than 1% in some of the components) than that of the normal stress.

Since the QT wave exhibits significant flux shift, shear stresses of 0.01, 0.02, 0.04, 0.08 and 1.0 GPa are applied and the corresponding flux shift is plotted for QT wave with respect to fiber orientation angle (Fig. 5), thus depicting that as the shear stress increases the flux shift also increases. This variation in flux shift of the QT wave is linear with applied shear stress.

To verify the flux shift predicted for QT wave in graphite/epoxy due to an applied shear stress by the acoustoelastic continuum theory, we use the finite element model to compute the flux shifts for QT wave. The graphite/epoxy plate is oriented in the x_1–x_3 plane with the fibers oriented at an angle of θ from the vertical direction (Fig. 6). The plate displacements are fixed to zero along the vertical boundaries in Fig. 6. The upper and lower horizontal boundaries are traction-free. The plate is modeled using a rectangular mesh of 4050 four-noded isoparametric elements with 90 elements in the horizontal direction and 45 elements are in the vertical direction. The constants used for the constant-average acceleration Newmark method are $\delta = 0.5$ and $\alpha = 0.25$ density of graphite/epoxy is taken as 1610 kg/m^3. After a preliminary parametric study (Section 3.2.1), it is determined that a minimum of 24 elements per wavelength simulate a transducer along the lower horizontal

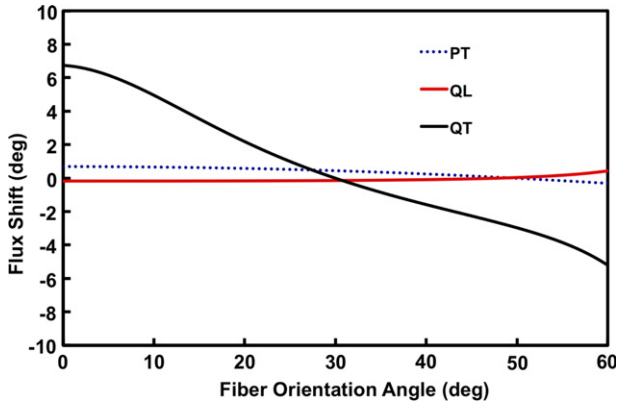

Fig. 3. Energy flux shift of QL, QT and PT waves in graphite/epoxy with respect to fiber orientation angle due to an applied shear stress of 0.1 GPa in the x_1–x_3 plane. The QT wave undergoes flux shift at 0° compared to QL and PT.

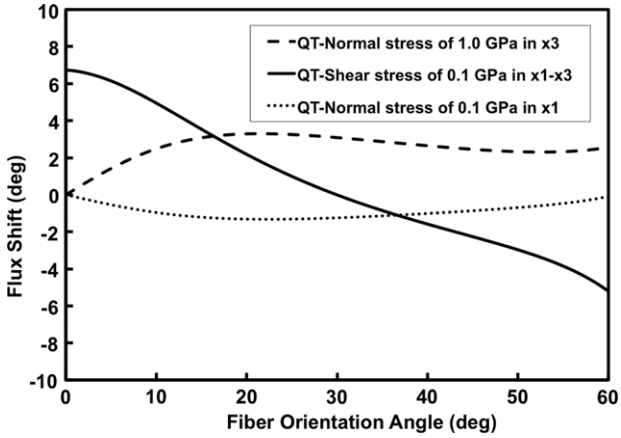

Fig. 4. Comparison of flux shift of QT wave due to an applied shear stress of 0.1 GPa with respect to flux shift in QT wave due to an applied normal stress of 0.1 GPa along x_1 axis and 1.0 GPa along x_3 axis. The applied shear stress case has higher flux deviation compared to applied normal stresses.

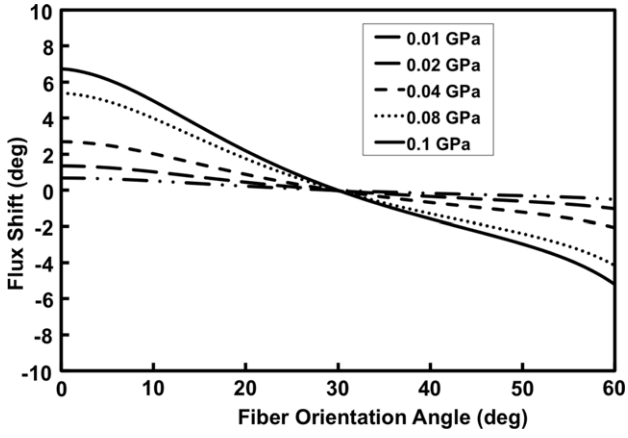

Fig. 5. Energy flux shift of QT wave in graphite/epoxy as a function of fiber orientation angle due to applied shear stress of 0.01, 0.02, 0.04, 0.08 and 1.0 GPa in the x_3–x_1 plane. The variation in flux shift is linear with the applied shear load.

boundary and 20 time increments per wave period would reduce wave dispersion such that results are valid for parametric studies used in this study. One cycle of sinusoidal displacements is imposed in the horizontal direction (“in plane pure transverse”) at 25 consecutive nodes along lower horizontal boundary of the plate for a time period of 2×10^{-05} s with a frequency of 50,000 cycles/s in order to flux more energy into the QT wave. The material properties used are given in Table 3. It is evident from Table 3 (column 3) that there are additional stiffness C^*_{ijkl} components due to the applied shear

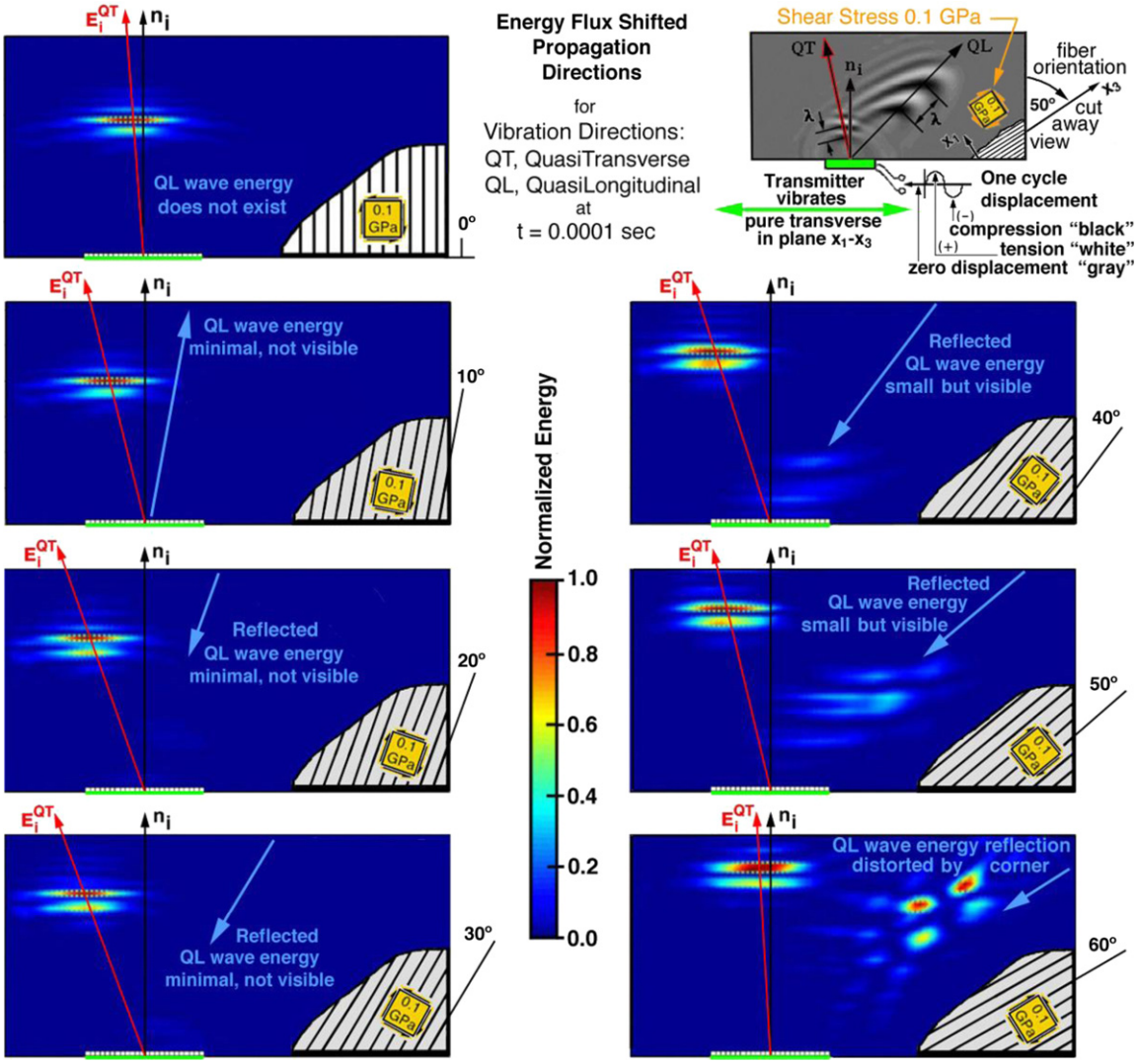

Fig. 6. Energy flux deviations including energy shift in unidirectional graphite/epoxy for various fiber orientations. Energy shift caused by a shear stress of 0.1 GPa applied to the fiber orientation is shown. Waves launched at the boundary use 24 elements per wavelength to minimize dispersion.

stress and these are incorporated in the finite element equations. These fourth order coefficients correspond to an applied shear stress of 0.1 GPa, this stress state corresponds to a high flux shift of 6.73° predicted by acoustoelastic theory. When the fourth order stiffness tensor C^*_{ijkl} is unsymmetric the finite element stiffness matrix is also unsymmetric. Finite element simulations are carried out for 0°, 10°, 20°, 30°, 40°, 50° and 60° fiber orientations for both zero stress state and applied shear stress state to determine the flux deviation angles and hence a stress-induced energy flux shift.

The QL wave is the fastest wave launched in the material and once it gets to the top surface it is reflected back. Because very little energy is transferred to the QL wave the QL wave is not predominantly observed in Fig. 6 for angles less than 50°. As observed from Fig. 6 the QT wave starts deviating towards the left side from the centerline of the transducer for fiber orientation angle from 0° to 30°. As the fiber orientation angle reaches 30° QT wave starts to deviate towards the centerline of the transducer. This observation is consistent with the acoustoelastic theory predictions (see Figs. 5 and 7).

It is obvious from Fig. 6 that for the fiber orientation of zero degrees energy flux deviation is not zero for the QT wave. The flux shift predicted by FEM is 6.8°. This validates the acoustoelastic theory prediction. The QT flux shift is determined for each 10° fiber orientation up to 60° and the results are plotted in Fig. 7. The FEM predicts the trend of flux shift for QT wave due to applied shear stress with reasonable accuracy. This is an independent confirmation of the energy flux shifts.

We believe that the predictions from this paper will be useful to develop and design new composite materials that can channel energy due to an applied stress. The methodology outlined in this paper will be useful to study several materials in nature e.g. rocks, which undergo high stress states and will have direct applications in petroleum industry. Novel structural materials/components can be developed for earthquake resistance. The design of these structures can be tailored further to guide the energy for optimum performance or flaw detection in nondestructive testing.

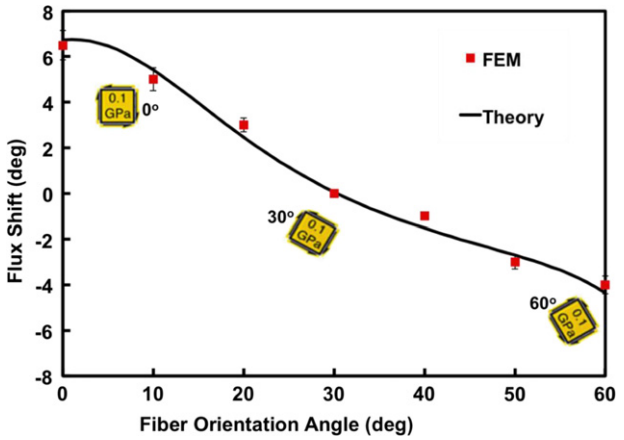

Fig. 7. Comparison of flux shifts predicted by acoustoelastic theory and FEM shows that the flux shifts for QT have a finite value at 0° fiber orientation. Inset shows loading at 0°, 30° and 60°.

5. Conclusions

In this paper we use the acoustoelastic theory and FEM to model the wave propagation in graphite/epoxy due to an applied shear stress. It is found out that the applied shear stress changes the anisotropy of graphite/epoxy hence leading to a shift in energy flux deviation. The flux deviation angles for zero stress were found for QL, QT and PT waves for fiber orientation angles from 0° to 60°. The energy flux shift for graphite/epoxy due to normal stress along x_1 and x_3 axes were also found and compared well with previous results. The flux shift of QL, QT and PT waves were found for the applied shear stress case. Important conclusions that can be drawn from the results are

(i) The QL and QT waves exhibit flux deviation in graphite/epoxy at zero shear stress due to the anisotropy of the material. Flux deviation of the PT wave is relatively small.
(ii) The application of normal stresses to graphite/epoxy leads to shifts in energy flux deviations for QL, QT and PT waves from the zero stress state, with QT waves having a larger shift compared to QL and PT waves.
(iii) The application of the shear stress also leads to shifts in the flux deviation in QL, QT and PT waves, but QT has a higher flux shift compared to QL and PT. The QT wave has significant flux shift at 0° and 60° due to the applied shear stress, where as the flux shift of QT wave under a normal stress from 0° to 60° is nearly zero.
(iv) The flux shift in QT wave due to applied shear stress is much higher than that of flux shift in QT wave due to normal stresses.
(v) The finite element model mesh density is tested for dispersion and it is determined that a minimum of 24 elements per wavelength at the simulated transducer boundary is required to approach the exact theoretical acoustoelastic predictions of shifts in energy flux deviation for various fiber orientations and loads.
(vi) The FEM prediction of the energy flux shift for QT wave under an applied shear stress for fiber orientation angles ranging from 0° to 60° independently confirms the acoustoelastic theory predictions.

Acknowledgments

AKN and RDK would like to thank Advanced Research Computing at Virginia Tech for support with High Performance Computing. AKN would like to acknowledge support from the Department of Mechanical Engineering, University of Arkansas.

Appendix

Expanding Eq. (3) for the case of shear stress = 0.1 GPa which leads to a shear strain of $\varepsilon_{31} = \varepsilon_{31} = 0.0095$. There are five linear elastic terms and ten nonlinear terms as expanded out in equations below.

$$\begin{aligned} K_{1113} &= C_{1113} + C_{3113}\varepsilon_{13} + C_{1313}\varepsilon_{13} + C_{1133}\varepsilon_{13} + C_{1111}\varepsilon_{31} + C_{111313}\varepsilon_{13} \\ &\quad + C_{111331}\varepsilon_{13} + C_{311313}\varepsilon_{13}\varepsilon_{13} + C_{311331}\varepsilon_{31}\varepsilon_{31} + C_{131313}\varepsilon_{13}\varepsilon_{13} + C_{131331}\varepsilon_{31}\varepsilon_{13} \\ &\quad + C_{113313}\varepsilon_{13}\varepsilon_{13} + C_{113331}\varepsilon_{31}\varepsilon_{13} + C_{111113}\varepsilon_{13}\varepsilon_{31} + C_{111131}\varepsilon_{31}\varepsilon_{31} \end{aligned} \tag{A.1}$$

$$\begin{aligned} K_{1131} &= C_{1131} + C_{3131}\varepsilon_{13} + C_{1331}\varepsilon_{13} + C_{1111}\varepsilon_{13} + C_{1133}\varepsilon_{31} + C_{113113}\varepsilon_{13} + C_{113131}\varepsilon_{31} \\ &\quad + C_{313113}\varepsilon_{13}\varepsilon_{13} + C_{313131}\varepsilon_{31}\varepsilon_{13} + C_{133113}\varepsilon_{13}\varepsilon_{13} + C_{133131}\varepsilon_{31}\varepsilon_{13} \\ &\quad + C_{111113}\varepsilon_{13}\varepsilon_{31} + C_{111131}\varepsilon_{31}\varepsilon_{31} + C_{113313}\varepsilon_{13}\varepsilon_{13} + C_{113331}\varepsilon_{31}\varepsilon_{13} \end{aligned} \tag{A.2}$$

$$K_{1313} = C_{1313} + C_{3313}\varepsilon_{13} + C_{1113}\varepsilon_{31} + C_{1333}\varepsilon_{13} + C_{1311}\varepsilon_{31} + C_{131313}\varepsilon_{13} + C_{131331}\varepsilon_{31} + C_{111313}\varepsilon_{31}\varepsilon_{31} + C_{111331}\varepsilon_{31}\varepsilon_{31} + C_{133313}\varepsilon_{13}\varepsilon_{13} + C_{133331}\varepsilon_{31}\varepsilon_{13} + C_{331313}\varepsilon_{13}\varepsilon_{13} + C_{331331}\varepsilon_{31}\varepsilon_{13} + C_{131113}\varepsilon_{13}\varepsilon_{31} + C_{131131}\varepsilon_{31}\varepsilon_{31} \quad (A.3)$$

$$K_{1331} = C_{1331} + C_{3331}\varepsilon_{13} + C_{1131}\varepsilon_{31} + C_{1311}\varepsilon_{31} + C_{1333}\varepsilon_{13} + C_{133113}\varepsilon_{13} + C_{133131}\varepsilon_{31} + C_{333113}\varepsilon_{13}\varepsilon_{13} + C_{333131}\varepsilon_{31}\varepsilon_{13} + C_{113113}\varepsilon_{13}\varepsilon_{31} + C_{113131}\varepsilon_{31}\varepsilon_{31} + C_{131113}\varepsilon_{13}\varepsilon_{31} + C_{131131}\varepsilon_{31}\varepsilon_{31} + C_{133313}\varepsilon_{13}\varepsilon_{13} + C_{133331}\varepsilon_{31}\varepsilon_{13} \quad (A.4)$$

Substituting values from Tables 1 and 2 into Eqs. (A.1)–(A.4), the values of coefficients are $K_{1113} = -0.64$ GPa (-0.64 GPa), $K_{1131} = -0.64$ GPa (-0.64 GPa), $K_{1313} = 5.24$ GPa (5.24 GPa) and $K_{1331} = 5.24$ GPa (5.24 GPa), where values in parentheses correspond to computer code used to compute these coefficients. The hand calculations carried out here validates the code used to compute the nonlinear elastic coefficients due to an applied stress.

References

[1] X.Y. Ao, C.T. Chan, Far-field image magnification for acoustic waves using anisotropic acoustic metamaterials, Phys. Rev. E 77 (2) (2008).
[2] J.S. Li, L. Fok, X.B. Yin, G. Bartal, X. Zhang, Experimental demonstration of an acoustic magnifying hyperlens, Nature Mater. 8 (12) (2009) 931–934.
[3] S. Guenneau, A. Movchan, G. Petursson, S.A. Ramakrishna, Acoustic metamaterials for sound focusing and confinement, New J. Phys. 9 (2007).
[4] H.Y. Chen, C.T. Chan, Acoustic cloaking in three dimensions using acoustic metamaterials, Appl. Phys. Lett. 91 (18) (2007).
[5] S.A. Cummer, D. Schurig, One path to acoustic cloaking, New J. Phys. 9 (2007).
[6] D. Torrent, J. Sanchez-Dehesa, Acoustic cloaking in two dimensions: a feasible approach, New J. Phys. 10 (2008).
[7] A.N. Norris, Acoustic cloaking theory, Proc. R. Soc. A 464 (2097) (2008) 2411–2434.
[8] C. Baron, Using the gradient of human cortical bone properties to determine age-related bone changes via ultrasonic guided waves, Ultrasound Med. Biol. 38 (6) (2012) 972–981.
[9] J.I. Katz, J.J. Hoffman, M.S. Conradi, J.G. Miller, Effective-medium theory of elastic waves in random networks of rods, Phys. Rev. E 85 (6) (2012).
[10] A. Vexler, I. Polyansky, R. Gorodetsky, Evaluation of skin viscoelasticity and anisotropy by measurement of speed of shear wave propagation with viscoelasticity skin analyzer, J. Invest. Dermatol. 113 (5) (1999) 732–739.
[11] A.E.H. Love, A Treatise on the Mathematical Theory Elasticity, Dover, New York, 1944.
[12] M.J.P. Musgrave, Crystal Acoustics, Holden-Day, San Francisco, 1970.
[13] R.E.J. Green, in: H. Herman (Ed.), Treatise on Materials Science and Technology, in: Ultrasonic Investigation of Mechanical Properties, vol. 3, Academic Press, New York, 1973.
[14] R.D. Kriz, W.W. Stinchcomb, Elastic-moduli of transversely isotropic graphite fibers and their composites, Exp. Mech. 19 (2) (1979) 41–49.
[15] W.H. Prosser, Ultrasonic Characterization of the Nonlinear Elastic Properties of Unidirectional Graphite/Epoxy Composites, Johns Hopkins University, Baltimore, MD, 1987.
[16] T. Tokuoka, Y. Iwashimizu, Int. J. Solids Struct. 4 (383) (1968).
[17] C.S. Man, W.Y. Lu, Towards an acoustoelastic theory for measurement of residual-stress, J. Elasticity 17 (2) (1987) 159–182.
[18] W.H. Prosser, R.D. Kriz, D.W. Fitting, Effect of stress on energy flux deviation of ultrasonic-waves in Gr/Ep composites, in: B.R. McAvoy (Ed.), IEEE 1990 Ultrasonics Symposium: Proceedings, vols. 1–3, 1990, pp. 961–964.
[19] A.D. Degtyar, S.I. Rokhlin, Absolute stress determination in orthotropic materials from angular dependences of ultrasonic velocities, J. Appl. Phys. 78 (3) (1995) 1547–1556.
[20] A.D. Degtyar, S.I. Rokhlin, Stress effect on boundary conditions and elastic wave propagation through an interface between anisotropic media, J. Acoust. Soc. Am. 104 (4) (1998) 1992–2003.
[21] Y.A. Zhuk, I.A. Guz, Influence of prestress on the velocities of plane waves propagating normally to the layers of nanocomposites, Internat. Appl. Mech. 42 (7) (2006) 729–743.
[22] W.J. Parnell, Effective wave propagation in a prestressed nonlinear elastic composite bar, IMA J. Appl. Math. 72 (2) (2007) 223–244.
[23] R.D. Kriz, Monitoring elastic stiffness degradation in graphite/epoxy composites, in: J.D. Achenbach, Y. Rajapakse (Eds.), Solid Mechanics Research for Quantitative Non-Destructive Evaluation, Martin Nijhoff Publishers, 1987, pp. 389–395.
[24] A.V. Amirkhizi, A. Tehranian, S. Nemat-Nasser, Stress-wave energy management through material anisotropy, Wave Motion 47 (8) (2010) 519–536.
[25] R.N. Thurston, Effective elastic coefficients for wave propagation in crystals under stress, J. Acoust. Soc. Am. 37 (2) (1965) 348–356.
[26] http://ntrs.nasa.gov/archive/nasa/casi.ntrs.nasa.gov/19930016913.pdf.
[27] J.N. Reddy, An Introduction to the Finite Element Method, second ed., McGraw-Hill International Editions, USA, 1993.
[28] K.J. Bathe, E.L. Wilson, Numerical Methods in Finite Element Analysis, Prentice-Hall, Englewood Cliffs, New Jersey, 1976.
[29] J.N. Reddy, Energy and Variational Methods in Applied Mechanics, John Wiley and Sons, New York, 1984.
[30] A.K. Nair, P.R. Heyliger, Elastic waves in combinatorial material libraries, Wave Motion 43 (7) (2006) 529–543.
[31] R.D. Kriz, P.R. Heyliger, Finite Element Model of Stress Wave Topology in Unidirectional Graphite/Epoxy: Wave Velocities and Flux Deviations, in: Review of Progress in Quantitative Nondestructive Evaluation, vol. 8A, 1989, pp. 141–148.
[32] R.D. Kriz, 2013. http://www.sv.vt.edu/classes/ESM5344/ESM5344_kriz_NoteBook/ESM5344_kriz.html.
[33] R.D. Kriz, H.M. Ledbetter, Elastic-wave surfaces in anisotropic media, Rheol. Anisotropic Mater. (1986) 79–92.